The Canadian Mineralogist
Vol. 45, pp. 293-305 (2007)

TASSIEITE, $(Na,\square)Ca_2(Mg,Fe^{2+},Fe^{3+})_2(Fe^{3+},Mg)_2(Fe^{2+},Mg)_2(PO_4)_6 \cdot 2H_2O$, A NEW HYDROTHERMAL WICKSITE-GROUP MINERAL IN FLUORAPATITE NODULES FROM GRANULITE-FACIES PARAGNEISS IN THE LARSEMANN HILLS, PRYDZ BAY, EAST ANTARCTICA

EDWARD S. GREW[§]

Department of Earth Sciences, University of Maine, 5790 Bryand Research Center, Orono, Maine 04469–5790, USA

THOMAS ARMBRUSTER

Laboratorium für chemische und mineralogische Kristallographie, Universität Bern, Freiestrasse 3, CH–3012 Bern, Switzerland

OLAF MEDENBACH

Institut für Geowissenschaften / Mineralogie, Ruhr-Universität Bochum, D–44780 Bochum, Germany

MARTIN G. YATES

Department of Earth Sciences, University of Maine, 5790 Bryand Research Center, Orono, Maine 04469–5790, USA

CHRISTOPHER J. CARSON

Research School of Earth Science, Australian National University, Canberra ACT 0200, Australia

ABSTRACT

Tassieite (IMA 2005–051), with an end-member formula $NaCa_2(Mg_2)(Fe^{3+}Mg)_{\Sigma 2}(Fe^{2+})_2(PO_4)_6 \cdot 2H_2O$, is a newly recognized Mg-dominant phosphate of the wicksite group. A representative composition derived with an electron microprobe is SiO_2 0.01, P_2O_5 44.54, SO_3 0.06, MgO 10.95, MnO 0.38, FeO 25.40 (meas.), FeO 14.93 (calc.), Fe_2O_3 11.63 (calc.), Na_2O 1.96, CaO 11.56, SrO 0.02, Y_2O_3 0.26, Ce_2O_3 0.08, Yb_2O_3 0.13, UO_2 0.04, F 0.04, H_2O 3.78 (calc.), sum 100.34 wt% (excluding F), which gives $Na_{0.60}Ca_{1.96}Mg_{2.59}Mn_{0.05}Fe^{2+}_{1.98}Fe^{3+}_{1.39}Y_{0.02}Yb_{0.01}S_{0.01}P_{5.98}O_{24} \cdot 2H_2O$ for 14 cations excluding Na, and 24 O; the Fe^{2+}:Fe^{3+} ratio is calculated from stoichiometry, and the H_2O, from ideal content. Overall, the analyses of all grains gave Na in the range 0.46–0.97 atoms per formula unit, and $X_{Mg} = Mg/(Mg + Fe^{2+})$ (atom ratio) is in the range 0.45–0.77 (for tassieite: $X_{Mg} > 0.5$). Single-crystal X-ray diffraction gives an orthorhombic symmetry, *Pbca*, *a* 12.4595(7), *b* 11.5955(16), *c* 12.7504(7) Å, *V* 1842.1(3) Å^3, calculated density 3.45 g/cm^3, $Z = 4$. The mineral is isostructural with wicksite, but with the *M*1 site dominated by Mg. Mg is the dominant divalent octahedrally coordinated cation in the structure, which is our rationale for recognizing tassieite as a distinct species. Indexed lines in the powder pattern [*d* in Å(*I*)(*hkl*)] are 6.40(5)(002), 3.497(40)(302), 3.000(80)(114), 2.895(80)(040), 2.735(100)(420,412), 2.545(10)(224) and 2.091(30)(106). The mineral is optically biaxial +, α 1.712(2), β 1.713(2), γ 1.722(2) (589 nm), 2*V* (meas.) 46(1)°, 2*V* (calc.) 37°. Pleochroism: *X* dark blue, *Y* blue, *Z* light brown; absorption: $X > Y >> Z$. Tassieite occurs in bands of secondary fluorapatite or in pseudomorphs of stornesite-(Y) within a fluorapatite nodule in a paragneiss specimen from between Johnston Fjord and Tassie Tarn (whence the name), Stornes Peninsula, Larsemann Hills, in Antarctica. Associated minerals are stornesite-(Y), wagnerite, xenotime-(Y), monazite-(Ce), pyrite, mélonjosephite and several unidentified Ca ± Na – Mg – Fe phosphates. Larger grains of tassieite (0.5–1 mm) show crystal faces and cleavage traces, but most grains (up to 0.3 mm) are platy and anhedral or irregular in outline. Tassieite seems to have formed hydrothermally from the alteration of stornesite-(Y) and wagnerite.

Keywords: phosphate, new mineral species, electron microprobe, crystal structure, Larsemann Hills, Antarctica.

§ *E-mail address*: esgrew@maine.edu

Sommaire

Nous décrivons la tassieïte (IMA 2005–051), phosphate de Mg récemment découvert faisant partie du groupe de la wicksite, et de composition idéale $NaCa_2(Mg_2)(Fe^{3+}Mg)_{\Sigma 2}(Fe^{2+})_2(PO_4)_6 \bullet 2H_2O$. Une composition représentative a été dérivée des mesures faites avec une microsonde électronique: SiO_2 0.01, P_2O_5 44.54, SO_3 0.06, MgO 10.95, MnO 0.38, FeO 25.40 (mes.), FeO 14.93 (calc.), Fe_2O_3 11.63 (calc.), Na_2O 1.96, CaO 11.56, SrO 0.02, Y_2O_3 0.26, Ce_2O_3 0.08, Yb_2O_3 0.13, UO_2 0.04, F 0.04, H_2O 3.78 (calc.), pour un total de 100.34% (poids, y exclue la teneur en F), ce qui donne une formule empirique $Na_{0.60}Ca_{1.96}Mg_{2.59}Mn_{0.05}Fe^{2+}_{1.98}Fe^{3+}_{1.39}Y_{0.02}Yb_{0.01}S_{0.01}P_{5.98}O_{24} \bullet 2H_2O$ pour 14 cations y exclue la teneur en Na, et 24 O; le rapport Fe^{2+}:Fe^{3+} est calculé à partir de la stoechiométrie, et la teneur en H_2O, de la formule idéale. En gros, les analyses de tous les grains indiquent entre 0.46 et 0.97 atomes de Na par formule unitaire, et X_{Mg} = Mg/(Mg + Fe^{2+}) (rapport d'atomes) varie dans l'intervalle de 0.45 à 0.77 (la définition de la tassieïte exige $X_{Mg} > 0.5$). La diffraction X sur monocristal indique une symétrie orthorhombique, *Pbca*, *a* 12.4595(7), *b* 11.5955(16), *c* 12.7504(7) Å, *V* 1842.1(3) Å^3, et une densité calculée de 3.45 g/cm^3, *Z* = 4. Le minéral possède la structure de la wicksite, mais avec Mg prédominant au site *M*1. Le Mg est le cation à coordinence octaédrique prédominant dans la structure, ce qui nous a poussé à proposer la tassieïte comme espèce distincte. Les raies indexées du spectre de diffraction (méthode des poudres) [*d* en Å(*I*)(*hkl*)] sont 6.40(5)(002), 3.497(40)(302), 3.000(80)(114), 2.895(80)(040), 2.735(100)(420,412), 2.545(10)(224) et 2.091(30)(106). Le minéral est biaxe +, α 1.712(2), β 1.713(2), γ 1.722(2) (589 nm), 2*V* (mes.) 46(1)°, 2*V* (calc.) 37°. Il est pléochroïque: *X* bleu foncé, *Y* bleu, *Z* brun pâle; absorption: *X* > *Y* >> *Z*. La tassieïte se trouve dans des rubans de fluorapatite secondaire ou en pseudomorphose de la stornesite-(Y) faisant partie d'un nodule de fluorapatite dans un specimen de paragneiss découvert entre Johnston Fjord et Tassie Tarn (d'où le nom), péninsule de Stornes, collines Larsemann, dans l'Antarctique. Lui sont associés stornesite-(Y), wagnérite, xénotime-(Y), monazite-(Ce), pyrite, mélonjosephite et plusieurs phosphates de Ca ± Na – Mg – Fe non identifiés. Les grains de tassieïte les plus gros (0.5–1 mm) montrent des faces et le tracé de clivages, mais la plupart des grains (jusqu'à 0.3 mm) sont en forme de plaquettes et xénomorphes. La tassieïte semble s'être formée en milieu hydrothermal par l'altération de la stornesite-(Y) et de la wagnérite.

(Traduit par la Rédaction)

Mots-clés: phosphate, nouvelle espèce minérale, microsonde électronique, structure cristalline, collines Larsemann, Antarctique.

Introduction

The wicksite group includes the hydrous calcic Fe-dominant phosphate *wicksite* (Sturman *et al*. 1981, Cooper & Hawthorne 1997) and its Mn-dominant analogue *bederite* (Galliski *et al*. 1999), as well as the isostructural hydrous Ca–Mn arsenate *grischunite* (Graeser *et al*. 1984, Bianchi *et al*. 1987). Galliski *et al*. (1999) further distinguished bederite from wicksite on the basis of the low occupancy of the site nearly fully occupied by Na in wicksite. We report here an Mg-dominant analogue of wicksite and bederite as the new mineral species *tassieite*. In contrast to wicksite and bederite, Na occupancy ranges from 46 to 97% in tassieite and varies independently of the Mg:Fe:Mn proportions, thereby introducing a complexity in defining wicksite-group minerals. Like wicksite and bederite, tassieite is a late-stage, low-temperature mineral, but its occurrence in Larsemann Hills paragneisses in Antarctica is uniquely restricted to a fluorapatite nodule containing stornesite-(Y) from its type locality (Grew *et al*. 2006).

The mineral and name were approved by the Commission on New Minerals and Mineral Names (CNMMN), International Mineralogical Association (2005–051). The name is for Tassie Tarn, a small triangular lake with a shape resembling that of Tasmania, 170 m south of the type and only locality, which was fixed at 69°24.929' S, 76°03.990' E on Stornes Peninsula, Larsemann Hills, Antarctica. The name has three syllables: tass-ee-ite. Holotype material (sample no. 113002A) is deposited in the National Museum of Natural History (Smithsonian Institution) as catalogue number NMNH 174436, the same as the holotype specimen for stornesite-(Y).

Analytical Methods

The optical properties were measured at the Ruhr-Universität Bochum by routine immersion procedure using a microrefractometer spindle-stage (Medenbach 1985). The precision of the measurements was restricted by the strong absorption of the crystals.

X-ray powder-diffraction data were obtained with a Gandolfi camera 57.3 mm in diameter and Cu*K*α radiation at the Ruhr-Universität (Table 1).

Cell dimensions were refined from reflections at scattering angles $13 < \theta < 20°$ obtained with graphite-monochromated Mo*K*α radiation on an ENRAF NONIUS CAD4 diffractometer equipped with a point detector at the University of Bern. CAD4 instrumentation gives higher accuracy albeit less precision than the CCD instrument.

Single-crystal X-ray-intensity collection of two crystal fragments (Fig. 1) was carried out with a three-circle SMART BRUKER CCD 1K at the University of Bern, graphite-monochromated Mo*K*α radiation (Table 2). The structure was solved by direct methods

in the standard space-group setting *Pbca* [*cf.* Cooper & Hawthorne (1997), who refined the structure of wicksite in *Pcab*], and refined with the program SHELXL–97 (Sheldrick 1997). Subsequently, the cation positions were numbered in the same sequence as adopted by Cooper & Hawthorne (1997). Scattering factors were assigned according to scattering power and bond lengths. All octahedral sites *M*1–*M*3 were refined with Mg and Fe assuming full occupancy. The *Ca* site was fixed at complete Ca occupancy, and the strongly distorted Na site was refined with partial Na occupancy. Both crystals gave almost identical results, which is not surprising, as both fragments originate from the same macrocrystal (Fig. 1). The coordinates and displacement parameters of the atoms are only given for the larger crystal #2 (Tables 3, 4). A table of structure factors is available from the Depository of Unpublished Data on the MAC web site [document tassieite CM45_293].

Tassieite and associated phosphates (Table 5) were analyzed with a Cameca SX100 electron microprobe at the University of Maine using wavelength-dispersive spectroscopy (WDS). Analytical conditions were:

TABLE 1. X-RAY POWDER-DIFFRACTION PATTERN OF TASSIEITE

I_{est}	d_{meas} (Å)	I_{calc}	d_{calc} (Å)	h k l
5	6.40	9	6.3752	0 0 2
5	5.99	--	--	--
40	3.497	19	3.4799	3 0 2
80	3.000	64	2.9841	1 1 4
80	2.895	64	2.8989	0 4 0
100	2.735	100	2.7439	4 2 0
			2.7206	4 1 2
10	2.545	15	2.5488	2 2 4
30	2.091	17	2.0948	1 0 6

Intensities are visual estimates. Calculated intensities and interplanar spacings are from LAZY PULVERIX (Yvon *et al.* 1977) using *a* 12.4595, *b* 11.5955, *c* 12.7504 Å obtained by single-crystal refinement.

TABLE 2. DETAILS OF THE SINGLE-CRYSTAL X-RAY REFINEMENTS OF TWO CRYSTALS OF TASSIEITE

Crystal reference (Fig. 1)	1	2
Space group	*Pbca*, No. 61	
a (Å)	12.4588(14)	12.4595(7)
b (Å)	11.5974(13)	11.5955(16)
c (Å)	12.7506(15)	12.7504(7)
V (Å^3)	1842.3(7)	1842.1(3)
Z	4	4
Calculated density (g/cm^3) from refined formula	3.407	3.415
Crystal size (mm)	0.03 × 0.05 × 0.08	0.14 × 0.06 × 0.08
Frame-exposure time (minutes)	5	1
2θ max (°)	56.27	55.94
h_{min}, h_{max}	-16, 15	-15, 15
k_{min}, k_{max}	-15, 10	-9, 15
l_{min}, l_{max}	-16, 13	-16, 16
Reflections measured	10665	11663
Unique reflections	2125	2100
Absorption correction	empirical	empirical
R_{σ}	0.0407	0.0865
R_{int}	0.0392	0.0582
Parameters refined	199	199
Reflections [I > 4σ(I)]	1622	1232
R(F) [I > 4σ(I)]	0.0329	0.0295
wR(F^2) (all)	0.0735	0.0483
$\Delta\rho_{min}$ (e. Å^{-3})	0.9 close to *M*3	0.6 close to *M*3
$\Delta\rho_{max}$ (e. Å^{-3})	0.9 close to *M*3	0.6 close to *M*3

TABLE 3. ATOM COORDINATES, OCCUPANCIES, AND B_{eq} VALUES FOR TASSIEITE CRYSTAL #2

site	*x*/*a*	*y*/*b*	*z*/*c*	B_{eq} (Å^2)	occupancy
P1	0.10935(7)	0.22866(9)	0.79975(9)	0.84(2)	1
P2	0.40130(7)	0.24099(8)	0.44377(9)	0.88(2)	1
P3	0.26527(7)	-0.02302(8)	0.6246(1)	0.91(2)	1
Fe1	0.15147(6)	-0.23132(8)	0.20756(8)	0.96(2)	0.316(3)
Mg1	0.15147(6)	-0.23132(8)	0.20756(8)	0.96(2)	0.684
Fe2	0.16801(5)	0.22717(5)	0.54175(6)	0.70(1)	0.684(3)
Mg2	0.16801(5)	0.22717(5)	0.54175(6)	0.70(1)	0.316
Fe3	0.01814(6)	-0.46041(6)	0.27722(7)	2.46(2)	0.657(3)
Mg3	0.01814(6)	-0.46041(6)	0.27722(7)	2.46(2)	0.343
Ca	0.23841(6)	0.00148(7)	0.37498(8)	1.17(1)	1
Na	0	-½	½	4.0(2)	0.463(7)
O1	0.0030(2)	0.2872(2)	0.7725(2)	1.07(5)	1
O2	0.0908(2)	0.1050(2)	0.8353(2)	1.16(5)	1
O3	0.1812(2)	0.2250(2)	0.7016(2)	1.03(5)	1
O4	0.1655(2)	0.3000(2)	0.8848(2)	0.92(5)	1
O5	0.3356(2)	0.2421(2)	0.5456(2)	0.90(5)	1
O6	0.1525(2)	-0.1832(2)	0.3613(2)	0.98(5)	1
O7	0.4087(2)	0.1158(2)	0.4060(2)	1.27(5)	1
O8	0.0122(2)	0.2062(2)	0.5333(2)	1.07(5)	1
O9	0.1906(2)	-0.4174(2)	0.2038(2)	1.18(5)	1
O10	0.1491(2)	-0.0415(2)	0.1891(2)	1.16(5)	1
O11	0.1984(2)	0.0557(2)	0.5523(2)	0.97(5)	1
O12	0.1745(2)	0.3960(2)	0.5494(2)	1.22(5)	1
OW	0.0268(2)	0.0091(3)	0.3788(3)	1.77(6)	1
H1	0.007(3)	0.056(3)	0.414(3)	1.4(12)	1
H2	-0.001(5)	-0.064(6)	0.394(5)	12.4(26)	1

Anisotropically refined atoms are given in the form of the isotropic equivalent displacement parameter defined as $B_{eq} = (8/3)\pi^2 \Sigma i(\Sigma j(U^{ij} a^{i*} a^{j*} a^{i}.a^{j})$. H1 and H2 were refined isotropically.

TABLE 4. ANISOTROPIC DISPLACEMENT PARAMETERS OF ATOMS FOR TASSIEITE, CRYSTAL #2

site	U_{11}	U_{22}	U_{33}	U_{12}	U_{13}	U_{23}
P1	0.0117(5)	0.0121(5)	0.0082(7)	0.0004(4)	-0.0005(5)	-0.0010(5)
P2	0.0118(5)	0.0137(6)	0.0079(7)	-0.0016(4)	0.0016(5)	0.0000(5)
P3	0.0142(5)	0.0121(5)	0.0084(5)	0.0007(4)	-0.0012(5)	0.0004(6)
*M*1	0.0124(5)	0.0166(6)	0.0075(6)	-0.0004(4)	0.0008(4)	-0.0017(4)
*M*2	0.0094(3)	0.0110(4)	0.0061(4)	-0.0001(3)	-0.0004(3)	0.0002(3)
*M*3	0.0374(5)	0.0149(5)	0.0412(7)	0.0055(4)	-0.0271(4)	-0.0045(4)
Ca	0.0176(4)	0.0158(4)	0.0110(4)	-0.0009(4)	0.0019(4)	-0.0018(4)
Na	0.041(4)	0.065(5)	0.047(5)	-0.018(3)	0.000(3)	0.033(3)
O1	0.012(1)	0.018(2)	0.011(2)	0.003(1)	-0.001(1)	-0.002(1)
O2	0.017(1)	0.014(2)	0.013(2)	-0.001(1)	-0.002(1)	0.004(1)
O3	0.012(1)	0.020(1)	0.007(2)	0.003(1)	0.000(1)	-0.001(1)
O4	0.013(1)	0.016(1)	0.006(2)	0.001(1)	0.000(1)	-0.002(1)
O5	0.014(1)	0.014(2)	0.007(2)	0.000(1)	0.003(1)	0.000(1)
O6	0.013(1)	0.016(2)	0.008(2)	0.001(1)	0.001(1)	0.003(1)
O7	0.019(1)	0.014(2)	0.016(2)	-0.001(1)	0.004(1)	-0.002(1)
O8	0.013(1)	0.017(1)	0.010(2)	0.003(1)	0.000(1)	0.001(1)
O9	0.018(1)	0.015(2)	0.012(2)	0.000(1)	0.003(1)	-0.001(1)
O10	0.018(1)	0.016(2)	0.010(2)	-0.002(1)	0.004(1)	0.004(1)
O11	0.015(1)	0.014(1)	0.008(2)	0.000(1)	-0.002(1)	0.000(1)
O12	0.021(1)	0.013(2)	0.012(2)	0.000(1)	-0.005(1)	-0.001(1)
OW	0.024(2)	0.017(2)	0.026(2)	0.006(2)	0.005(2)	-0.001(2)

accelerating voltage 15 kV, beam current 10 nA, count time 5s, and spot diameter 5 μm (except 20 μm for the second crystal, used for refinement of the structure), and the data were processed using the X-Phi correction of Merlet (1994). We used the following standards for the phosphates: fluorapatite (F*K*α), tugtupite (Na*K*α), synthetic $Mg_3(PO_4)_2$, (Mg*K*α), albite (Al*K*α), albite (Si*K*α), fluorapatite or synthetic $Mg_3(PO_4)_2$ (P*K*α), barite (S*K*α), tugtupite (Cl*K*α), fluorapatite (Ca*K*α), rutile (Ti*K*α), rhodonite (Mn*K*α), almandine (Fe*K*α), celestine (Sr*L*α), synthetic Y–Al garnet (Y*L*α), synthetic REE phosphates (REE *L*α), and U metal (U*M*β). We attempted analyses at 20 spots per grain, where each constituent was counted for 5 seconds. However, after culling the results because of impurities and allowing for compositional zoning, compositions of tassieite are averages of 6 to 20 spots per grain or zone in a grain.

A potential problem with electron-microprobe analyses of minerals for Na, particularly in cases of hydrous minerals, is migration of Na during course of the analyses (*e.g.*, Autefage 1980, Autefage & Couderc 1980). The migration can be minimized by reducing analytical time, accelerating voltage and sample current, by increasing beam diameter and by moving the sample under the beam. For example, Autefage & Couderc (1980) reported negligible Na migration in albite using a beam 20 μm in diameter for three minutes at 15 kV, 50 nA sample current and fixed sample, but Na started to migrate within 10 seconds under these conditions with a beam 5 μm in diameter. Autefage (1980) recommended an accelerating voltage of 10 kV, a sample current of 30 nA, a beam at least 10 μm in diameter, and sample movement. Because of the small size of most grains of tassieite and an abundance of inclusions in these grains, we had to find a balance between minimally damaging operating conditions and a clean area on the grain large enough to analyze, whence our choice of a beam 5 μm in diameter for most tassieite grains. Our conditions were less conducive to Na migration than those used in other studies of wicksite-group minerals for which operating conditions were given in detail: 15 kV accelerating voltage, 20 nA sample current, 20 s counting time on peak for wicksite (Cooper & Hawthorne 1997, Oberti *et al.* 1993). Galliski *et al.* (1999) used the same conditions for bederite, but also gave the beam size as 5 μm. In both cases, Na content determined by electron-microprobe analyses was found to agree with Na content calculated from the crystal-structure refinement. In summary, we conclude that significant Na migration was unlikely under the conditions we used, and certainly no more than in other studies of wicksite-group minerals.

Identification of several minerals not analyzed with WDS was confirmed by taking an element scan using energy-dispersive spectroscopy (Table 5).

TABLE 5. MINERALS ENCLOSED IN FLUORAPATITE IN SAMPLE 113002A

Position in nodule	Core	Margin	Analysis
Stornesite-(Y) (Sto)[‡]	×	×	
Fluorapatite (Fap)[‡]	host	host	
Wagnerite (Wag)[‡]	×	×	
Quartz (Qtz)	–	×	
K-feldspar (Kfs)[‡]	–	×	
Biotite (Bt)	–	×	
Monazite-(Ce) (Mnz)	×	×	EDS[†]
Xenotime-(Y) (Xnt)	×	×	EDS, WDS[§]
Pyrite (Py)	×	–	EDS
Magnetite (Mgt)	2nd	–	
Fluorapatite (veins and margins)	2nd	2nd	WDS
Tassieite (Tss)	2nd	–	WDS
Mélonjosephite (Mj)	2nd	–	WDS
Jahnsite-like (Jhn)	2nd	--	WDS
Unid. Ca-Mg-Fe phosphate	2nd	--	WDS
Lazulite–souzalite-like	2nd	2nd	EDS
Cassiterite (Cst)	2nd	–	EDS

[‡] Analytical data given in Grew *et al.* (2006); [†] Qualitative analysis using energy-dispersive spectroscopy. [§] Quantitative analysis using wavelength-dispersive spectroscopy. ×: present; 2nd: present only as a secondary mineral.

Occurrence, Associated Minerals and Origin

Tassieite occurs in a single, rounded nodule ~8–10 cm across of dark brown fluorapatite in biotite – quartz – plagioclase paragneiss, a distinctive lithologic unit characterized by segregations of cordierite, prismatine, grandidierite and tourmaline (Carson *et al.* 1995a, Ren *et al.* 2003). A zone of plagioclase gneiss not exceeding 1 cm in thickness and containing abundant wagnerite and minor apatite and quartz surrounds the nodule, which is mantled by a discontinuous corona of wagnerite.

Tassieite was found only in the core of the fluorapatite nodule. It is not present either in the margin of the nodule or in the other two samples containing stornesite-(Y) (113002C, 121401E, Grew *et al.* 2006), and none has been found in the vicinity of K-feldspar, biotite or quartz. Except for secondary fluorapatite, tassieite is the most abundant secondary mineral in the core of the nodule. It occurs either in bands of secondary fluorapatite typically turbid with fine inclusions (Fig. 1) or in pseudomorphs of stornesite-(Y) (Figs. 2a, b); it also replaces wagnerite (Figs. 2c, d). A few larger grains of tassieite (*i.e.,* 0.5–1 mm) show crystal faces and cleavage traces (*e.g.*, Fig. 1), but most grains, which are 0.02 to 0.3 mm in longest dimension, are platy and anhedral (Figs. 2a, b). Tassieite commonly shows a faint zoning in back-scattered electron images, but it is rarely regular (Figs. 2d, 3b). Tassieite in places encloses xenotime-(Y) (Fig. 3a), in one case, as abundant, fine particles (Fig. 3b).

The other secondary minerals in the bands and pseudomorphs are phosphates; several of these could not be definitively identified owing to their very fine grain-size and relative scarcity (indicated by the suffix "-like" in Table 5). Secondary fluorapatite differs from primary fluorapatite in being very fine-grained (*e.g.*, Fig. 2d), and compositionally heterogeneous. On average,

TABLE 6. COMPOSITIONS OF MISCELLANEOUS SECONDARY PHOSPHATES

Sample	113002 A	113002 A	113002 A	113002 A	113002 A	113002 A	113002 A	113002 A	112906 H2[¶]	120302 C[#]	113002 C*
Mineral	Fap	Fap	Fap	Mj	Mj	Jhn	Jhn	Unid	Isk	Isk	Isk-like
Grain	a1	aa1	aa2	Area 1[‡]	Area 4[†]	7[§]	1—6	9			
No. spots	20	20	20	20	20	19	7	20	19	18	9
SiO_2 wt%	b.d.	b.d.	b.d.	0.01	0.01	0.02	b.d.	0.04	b.d.	0.02	0.02
P_2O_5	42.20	41.65	42.28	41.01	41.76	33.63	33.81	43.84	39.31	38.93	38.33
SO_3	0.01	0.02	0.03	0.01	0.04	b.d.	0.03	0.03	0.03	0.04	0.51
TiO_2	0.01	b.d.	b.d.	b.d.	0.01	b.d.	b.d.	b.d.	0.38	0.22	b.d.
Al_2O_3	b.d.	b.d.	b.d.	b.d.	0.05	b.d.	b.d.	b.d.	0.04	0.01	b.d.
Fe_2O_3	--	--	--	21.54	19.78	18.22	19.56	--	--	--	--
MgO	b.d.	0.06	b.d.	3.80	3.95	7.70	8.07	28.47	22.79	22.75	19.64
MnO	0.23	0.25	0.21	0.04	0.04	0.30	0.23	0.10	b.d.	0.01	0.06
FeO	0.67	0.82	0.72	14.47	15.35	8.66	7.85	–	0.13	0.07	1.06
Na_2O	0.02	0.23	0.01	b.d.	0.01	0.37	0.90	0.73	0.01	0.02	0.25
CaO	54.40	52.67	53.22	16.09	16.23	7.84	6.23	2.41	31.31	31.51	29.40
SrO	b.d.	0.04	0.01	0.02	0.01	0.02	b.d.	b.d.	b.d.	b.d.	0.11
Y_2O_3	0.04	0.42	0.30	b.d.	b.d.	b.d.	0.49	0.45	b.d.	b.d.	1.51
La_2O_3	b.d.	0.08	0.03	0.01	0.01	b.d.	b.d.	b.d.	b.d.	0.05	b.d.
Ce_2O_3	0.01	0.22	0.08	b.d.	b.d.	b.d.	0.01	b.d.	0.03	0.01	0.01
Nd_2O_3	0.05	–	–	b.d.	b.d.	0.02	0.03	0.01	0.05	b.d.	–
Tm_2O_3	0.03	–	–	b.d.	b.d.	b.d.	b.d.	b.d.	b.d.	0.05	–
Yb_2O_3	0.04	0.02	1.47	0.05	b.d.	0.28	0.11	0.16	0.02	0.03	0.29
UO_2	b.d.	b.d.	b.d.	b.d.	b.d.	0.01	b.d.	0.02	0.01	b.d.	0.01
F	2.93	3.35	3.07	0.05	0.03	0.01	0.01	0.02	10.57	10.28	8.35
Cl	0.77	0.59	0.62	b.d.	b.d.	0.02	0.04	0.01	b.d.	b.d.	0.04
H_2O calc	0.18	0.02	0.15	2.58	2.59	18.99	19.13	–	0.03	0.13	0.89
O=F	-1.23	-1.41	-1.29	-0.02	-0.01	0.00	-0.01	-0.01	-4.45	-4.33	-3.52
O=Cl	-0.17	-0.13	-0.14	0	0	-0.01	-0.01	0.00	0	0	-0.01
Sum	100.17	98.89	100.76	99.66	99.88	96.08	96.48	92.11	100.28	99.80	96.97
FeO meas	0.67	0.82	0.72	33.85	33.15	25.06	25.45	15.82	0.13	0.07	1.06
Formulae per O and total cations											
O anhyd.	12.5	12.5	12.5	8.5	8.5	17	17		4.5	4.5	4.5
Cations	--	--	--	5	5	10	10		--	--	--
Si *apfu*	0	0	0	0.001	0.001	0.003	0		0	0.001	0.001
P	3.007	3.011	3.016	2.018	2.043	4.045	4.039		0.988	0.984	1.002
S	0.001	0.001	0.002	0	0.002	0	0.003		0.001	0.001	0.012
Ti	0	0	0	0	0.001	0	0		0.008	0.005	0
Al	0	0	0	0	0.003	0	0		0.001	0.001	0
Fe^{3+}	–	–	–	0.942	0.860	1.948	2.077		–	–	–
Mg	0	0.008	0	0.330	0.341	1.631	1.697		1.008	1.013	0.904
Mn	0.016	0.018	0.015	0.002	0.002	0.036	0.027		0	0	0.002
Fe^{2+}	0.047	0.058	0.051	0.703	0.742	1.029	0.926		0.003	0.002	0.027
Na	0.003	0.038	0.001	0	0.001	0.101	0.247		0.001	0.001	0.015
Ca	4.906	4.819	4.805	1.002	1.005	1.193	0.942		0.996	1.008	0.973
Sr	0	0.002	0.001	0.001	0	0.002	0		0	0	0.002
Y	0.002	0.019	0.013	0	0	0	0.036		0	0	0.025
La	0	0.002	0.001	0	0	0	0		0	0	0
Ce	0	0.007	0.002	0	0	0	0		0	0	0
Nd	0.002	--	--	0	0	0.001	0.002		0.001	0	--
Tm	0.001	--	--	0	0	0	0		0	0	--
Yb	0.001	0.001	0.038	0.001	0	0.012	0.005		0	0	0.003
U	0	0	0	0	0	0	0		0	0	0
Sum	7.986	7.985	7.945	5	5	10	10		3.007	3.016	2.966
F	0.779	0.905	0.818	--	--	--	--		0.993	0.971	0.816
Cl	0.109	0.085	0.089	0	0	–	–		0	0	0.002
H_{calc}	0.112	0.010	0.093	1	1	18	18		0.007	0.029	0.182
Sum	1	1	1	1	1	18	18		1	1	1

Fe as FeO unless Fe_2O_3 calculated by stoichiometry. No. spots: number of spots where elements were counted for 5 s. b.d.: below detection. –: not analyzed or not calculated. H_2O calculated from stoichiometry: F + Cl + H = 1 except Jh, where H = 18. [‡] Fig. 3d. [†] Fig. 3c. [§] Fig. 4. [¶] An alteration product of wagnerite from 250 m east of tassieite locality. [#] An alteration product of wagnerite from base of Gneiss Peak, 500 m ENE of tassieite locality. [*] An alteration product of stornesite-(Y) from the tassieite locality. Symbols: Fap: fluorapatite, Isk: isokite, Jhn: jahnsite-like mineral, Mj: mélonjosephite, Unid: unidentified Ca–Mg–Fe phosphate.

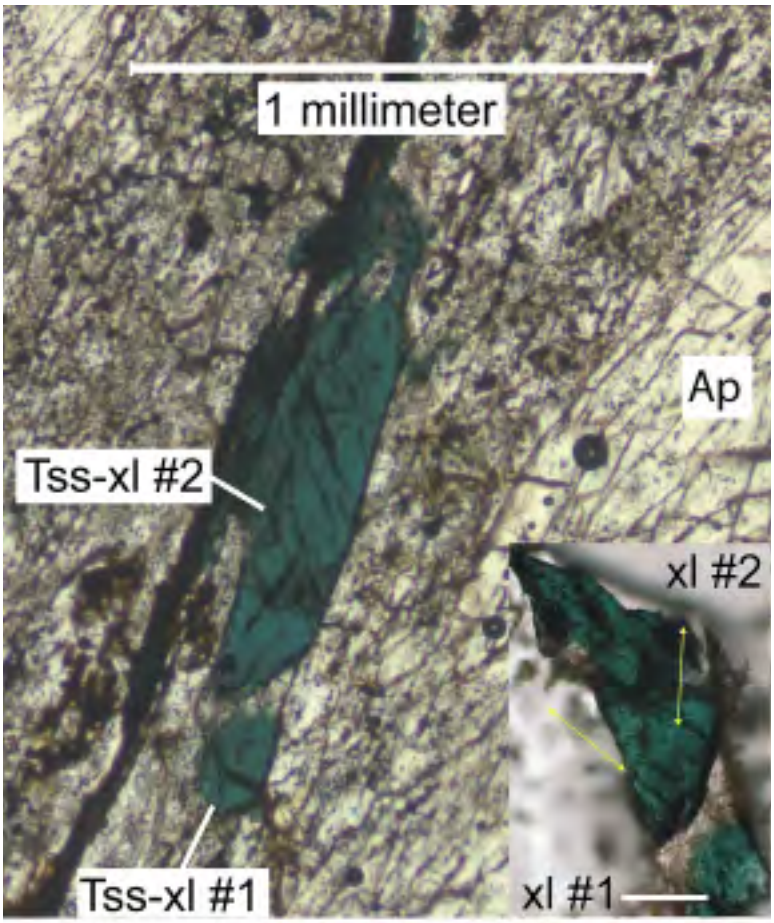

FIG. 1. Photomicrograph (plane-polarized light) of tassieite in a band of alteration (abundant particles) cutting fluorapatite (Ap). Fragments of the two crystals were used for single crystal and Gandolfi X-ray diffraction, optical studies and electron-microprobe analyses. Inset shows portions of the crystals (enlarged) after extraction to illustrate two cleavages (yellow arrows) in tassieite. Sample 113002A.

secondary fluorapatite contains less Cl, Mg, and Fe; Na, Y and Yb contents are erratic (Table 6). Xenotime-(Y) is widespread as fine particles (*e.g.,* Figs. 2c, 3b), whereas monazite-(Ce) is less common, albeit in places coarser (Fig. 3c). An average of WDS electron-microprobe analyses of two xenotime-(Y) grains is $(Ca_{0.01}Sc_{0.001}Y_{0.77}Ce_{0.001}Nd_{0.005}Sm_{0.008}Gd_{0.02}Tb_{0.006}Dy_{0.06}Ho_{0.01}Er_{0.04}Tm_{0.008}Eu_{0.002}Yb_{0.04}Lu_{0.003}U_{0.002})\ Si_{0.001}P_{1.00}O_4$. Mélonjosephite is pleochroic from very dark green (nearly opaque) to brown and is best distinguished from tassieite in back-scattered-electron (BSE) images, as it is lighter (Figs. 2c, 3c, 3d). Grains show some compositional heterogeneity, but on average, the composition of mélonjosephite (Table 6) closely matches the ideal formula $Ca(Mg,Fe^{2+})Fe^{3+}(PO_4)_2(OH)$ (Fransolet 1973). Birefringent brown phases form either fine-grained aggregates ("unid" in Fig. 3c) or tufted plates ("Jhn" in Fig. 4). In some cases, their compositions approximate that of what could be an Mg-dominant, Mn-poor jahnsite-group mineral. However, the analyses give total Mg + Mn + Fe^{2+} contents (Table 6) less than expected in the formula of such a mineral: $CaFe^{2+}(Mg,Fe^{2+})_2Fe^{3+}{}_2(PO_4)_4(OH)_2{\bullet}8H_2O$ (Moore 1974). Other brown phosphates give a different composition altogether (Table 6), or are too heterogeneous to give a meaningful average. A blue-green pleochroic mineral could be either lazulite or souzalite; a semiquantitative energy-dispersion spectroscopy (EDS) analysis in section 121401E described by Grew *et al*. (2006) gave an approximate composition (Mg, Fe):Al:P ≈ 2:3:3, consis-

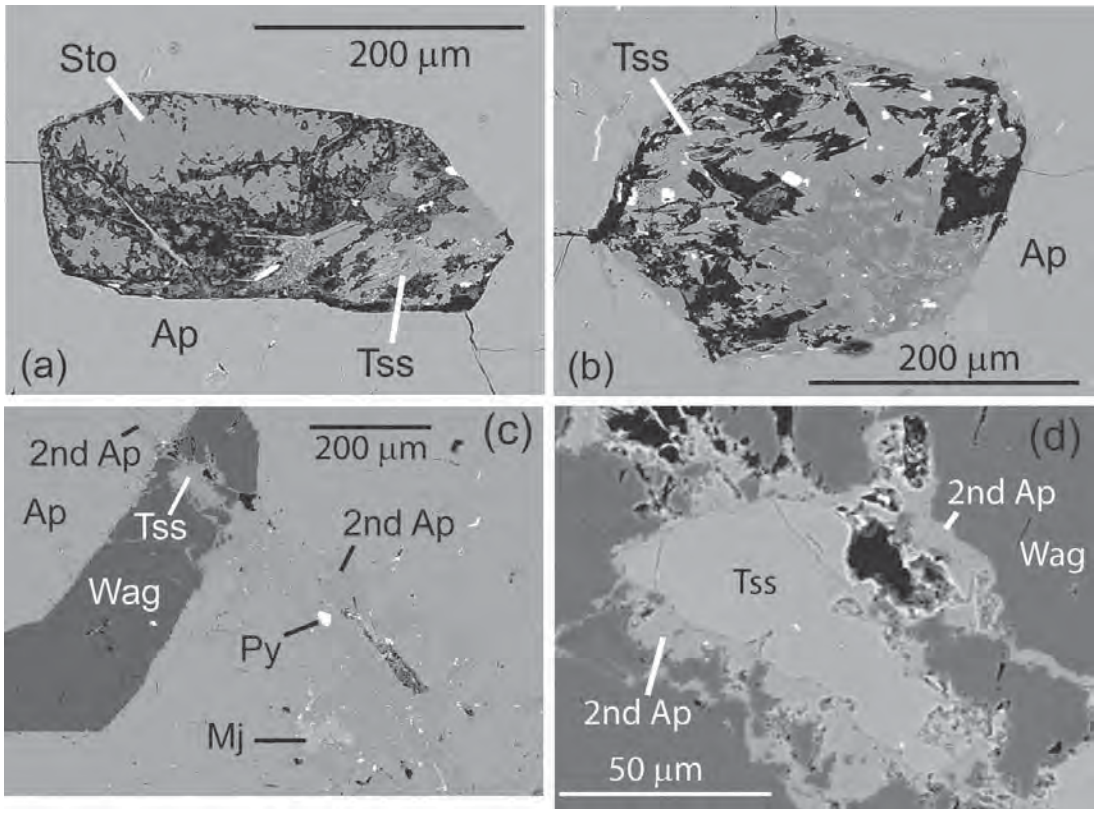

FIG. 2. Back-scattered-electron images of tassieite (Tss) and associated secondary minerals in sample 113002A. (a) and (b) Fluorapatite (Ap) enclosing a pseudomorph of stornesite-(Y), with one relic preserved (Sto). The white grains are xenotime-(Y). The areas slightly darker than tassieite in (b) are the jahnsite-like mineral. (c) Tassieite grain mantled in secondary fluorapatite at intersection where band of secondary fluorapatite (2nd Ap) crosses a wagnerite grain (Wag) in primary fluorapatite (Ap), which is slightly lighter than secondary fluorapatite. Mélonjosephite (Mj) is also present (Table 6, area 1). The bright spots in the band are dominantly xenotime-(Y); monazite-(Ce) is less abundant, and pyrite (Py) is rare. (d) Enlargement of tassieite grain showing indistinct zoning.

tent with either mineral. Like tassieite, mélonjosephite and the jahnsite-like mineral have not been found near silicates, whereas the lazulite–souzalite-like mineral is more commonly seen with K-feldspar.

Tassieite, mélonjosephite and the jahnsite-like mineral are inferred to have formed from low-temperature alteration of stornesite-(Y), wagnerite and fluorapatite, a paragenesis similar to pegmatitic occurrences of "wicksite-like" minerals and mélonjosephite (Peacor *et al*. 1985, Fransolet *et al*. 1985, Povondra *et al*. 1987). The presence of stornesite-(Y) is essential; wagnerite, a widespread phosphate in the Larsemann Hills, by itself or with fluorapatite, does not suffice for tassieite formation. We attribute the alteration to late hydrothermal activity associated with faulting. Brittle faults postdating regional metamorphism and deformation have been reported in the Larsemann Hills (Dirks *et al*. 1993, Carson *et al*. 1995b). Evidence for such late alteration are chloritization and epidote-bearing fractures along a prominent lineament bounding Blair Bay, 2.5 km northeast of the tassieite locality, one of several lineaments that Stüwe *et al*. (1989) mapped in the Larsemann Hills using aerial photography. Halogen and silica activities in the hydrothermal fluids were sufficiently low to stabilize hydrous Ca ± Na – Mg – Fe phosphates. Isokite, $Ca(Mg,Fe)PO_4(F,OH)$, or an isokite-like mineral, both of which are found in other samples from the Larsemann Hills as an alteration of wagnerite or stornesite-(Y) (Table 6), could be due to higher activities of fluorine. At higher activities of silica, more Mg and Fe are incorporated in silicate minerals, leaving less for phosphates. The high $Mg:Fe^{2+}$ ratio and low Mn content of tassieite reflect the relative proportions of Mg, Fe and Mn in stornesite-(Y) and

wagnerite, which have created a more magnesian environment than those in which the other wicksite-group minerals were found. Wicksite occurs in nodules with the Fe phosphates wolfeite, satterlyite and marićite as well as Fe–Mn-bearing alluaudite-group minerals in ironstone and shale (Sturman *et al.* 1981, Robertson 1982, Robinson *et al.* 1992). Bederite and Mn-bearing "wicksite-like" minerals occur in pegmatites and a high-alumina phosphate deposit; associated minerals include, respectively, Fe–Mn phosphates, *e.g.*, barbosalite, and the Al phosphates gatumbite, augelite, burangaite and trolleite (Peacor *et al.* 1985, Ek & Nysten 1990, Galliski *et al.* 1999). Except for the trace amount of cassiterite, there is little definitive evidence for the metasomatic introduction of elements during the hydrothermal alteration at the tassieite locality: Y and the rare-earth elements for secondary xenotime-(Y) and monazite(Ce) could have been released during breakdown of fluorapatite and stornesite-(Y).

Physical and Optical Properties of Tassieite

Tassieite is dark green with a very light green streak and a vitreous luster. Its hardness cannot be determined because of the small grain-size and the very limited amount of available material, *i.e.*, only a few crystals exclusively in thin sections. Tassieite is brittle. It has two cleavages: good to perfect on {100}; a second intersects this at an angle of 60° (Fig. 1). The density calculated from the formula based on the electron-microprobe data (see below) for the second crystal used for structure refinement, is 3.45 g/cm^3.

Grains in thin section are transparent (Fig. 1). Tassieite is optically biaxial positive, α 1.712(2), β

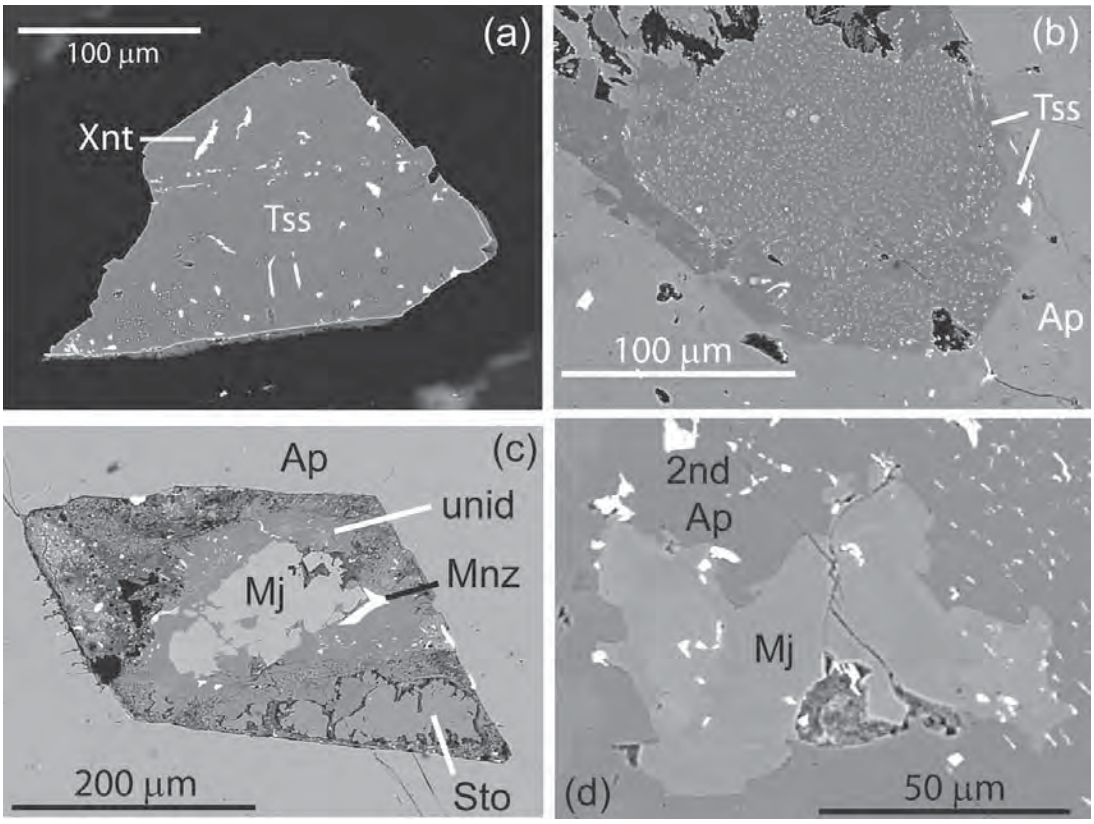

Fig. 3. Back-scattered-electron images of tassieite (Tss) and mélonjosephite (Mj) in sample 113002A. (a) Xenotime-(Y) (Xnt) in tassieite broken from crystal 2 in Figure 1. (b) Very fine-grained xenotime-(Y) (bright spots) in zoned tassieite in area 9 (Table 9). (c) Mélonjosephite (Mj) in area 4 (Table 6); a pseudomorph of stornesite-(Y) in fluorapatite (Ap) with one relic preserved (Sto). The large white grain is monazite-(Ce), but the finer white grains and specks are mostly xenotime-(Y); cassiterite and pyrite also are present. The unidentified mineral surrounding mélonjosephite is a heterogeneous Na-Ca-Mg-Fe phosphate. (d) Mélonjosephite (Mj) in area 1 (Table 6); enlargement of Figure 2c shows zoning in mélonjosephite. The white grains are mostly xenotime-(Y); a few are monazite-(Ce). 2nd Ap: secondary fluorapatite.

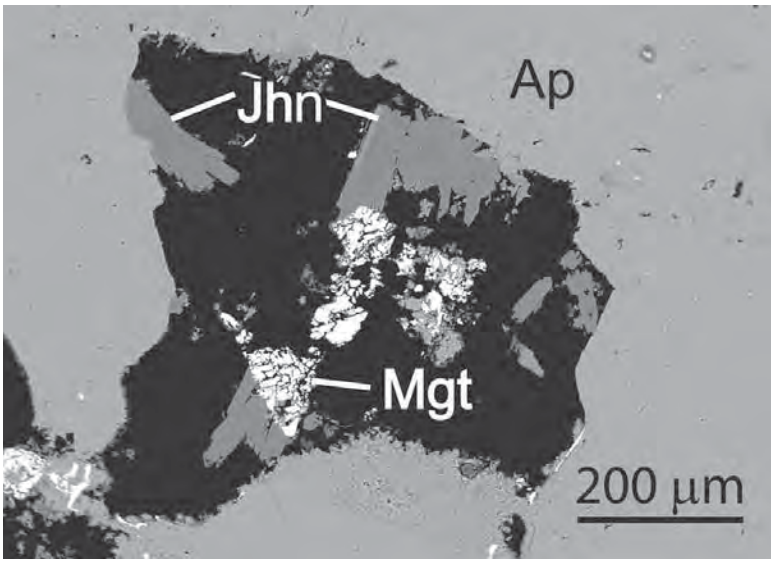

FIG. 4. Back-scattered-electron image of area 7 showing jahnsite-like mineral (Jhn) in Table 6. Sample 113002A.

1.713(2), γ 1.722(2) (589 nm), with 2*V* (meas.) = 46(1)°, 2*V* (calc.) = 37°. Dispersion is very weak. Pleochroism is marked, with *X* dark blue, *Y* blue, *Z* light brown; the absorption is $X > Y >> Z$. Fluorescence was not observed.

CRYSTALLOGRAPHIC PROPERTIES

Tassieite is isostructural with wicksite and bederite. However, in contrast with these two minerals, Mg is the dominant octahedrally coordinated divalent cation in the structure. The *M*1 site is 68–69% occupied by Mg (Table 7). Charge balance requires the presence of 1.523–1.537 Fe^{3+} per formula unit. Given the relative sizes of the *M* sites (Table 8) and following Cooper & Hawthorne (1997), we have assumed that all Fe at *M*2 is Fe^{3+}. The remainder is assigned to the second smallest site, *M*1. Note that Fe^{3+} was not reported at *M*1 in either wicksite (Cooper & Hawthorne 1997) or bederite (Galliski *et al.* 1999). If we were to assume the Na content measured with the electron microprobe instead of the refined Na content, the calculated Fe^{3+} occupancy at *M*1 would drop from 0.168 to 0.028 atoms per formula unit in crystal #2. The *M*3 site is the largest and most distorted octahedron in the structure, and it is doubtful that Fe^{3+} is present or that Mg could ever be dominant.

The *Ca* site is fully occupied by 20 electrons, *i.e.,* measurable amounts of constituents other than Ca are absent. The *Na* site is 46–48% occupied by Na. The positions of both proton sites could be refined, confirming the presence of two H_2O molecules. The presence of OH in tassieite can be excluded. All O sites involve bonds to P and at least two *M* cations except O8, which is bonded only to P2 and *M*2. A simple calculation gives a valence sum of 1.7 for O8. However, the *M*2–O8 bond length is the shortest octahedral bond in the structure (Table 8), and O8 accepts strong hydrogen bonds from the H_2O molecule; thus the apparent underbonding is adjusted by reduction of the bond lengths.

There is good agreement between the composition based on the refinement and the results of the electron-microprobe analysis for P, Ca, Mg, and total Fe in crystal #2 (Table 9). In contrast, the discrepancy between the refined Na occupancy and the electron-microprobe-inferred Na content exceeds the uncertainty of either measurement. Because refinements of both crystals gave nearly identical Na contents, the discrepancy cannot be dismissed as a result of zoning, despite the wide variation in Na content between other analyzed grains (see below). If a larger amount of Na is assumed to occupy the *Na* site, *e.g.*, 0.624 atoms per formula unit (*apfu*), displacement parameters become unrealistically large, and *R*1 increases by 0.3%.

In an alternative model in full agreement with the Na concentration determined by electron-microprobe analyses, we assume additional 0.14 *apfu* Na at *M*3, corresponding to a Na occupancy of 0.07%. Scattering factors of Na and Mg are very similar, and these elements are difficult to distinguish, particularly where present as minor components. Minor Na at *M*3 would require the same amount of Fe^{2+} at *M*1 to be interpreted as ferric iron for charge balance. The agreement between the refined and measured MgO is improved in

this model, but the difference in calculated Fe^{3+}:Fe^{2+} ratio is increased owing to the different normalizations used (Table 9).

Chemical Composition and Compatibility Index of Tassieite

Tassieite is highly variable in composition from grain to grain (*e.g.*, Table 9), and some individual grains appear indistinctly zoned in back-scattered-electron images (Figs. 2d, 3b). The principal variables are Mg (8.60–15.99 wt.% MgO), Fe (17.03–27.75 wt.% expressed as FeO), and Na (1.63–3.16 wt% Na_2O), resulting in X_{Mg} = Mg/(Mg + Fe^{2+}) in the range 0.445–0.769 (Fig. 5a). The Fe^{3+} contents were calculated assuming full occupancy of the *Ca*, *M* and *P* sites and absence of Na at *M*3, that is, 14 total cations excluding Na, and 24 O excluding H_2O. If Na were to occupy the *M*3 site, then this calculation would give too low a Fe^{3+}:Fe^{2+} ratio, *e.g.,* assuming 0.14 Na at *M*3 increases the calculated proportion of Fe^{3+} from 0.46 to 0.51 (Table 9).

TABLE 7. CATION ASSIGNMENT IN THE TWO STRUCTURE REFINEMENTS OF TASSIEITE

	P	Fe^{tot}	Fe^{3+}	Fe^{2+}	Mg	Ca	Na	H	Sum
First crystal									
*P*1	1								1.000
*P*2	1								1.000
*P*3	1								1.000
*M*1		0.315(4)	0.092	0.223	0.685				1.000
*M*2		0.669(4)	0.669		0.331				1.000
*M*3		0.643(5)		0.643	0.357				1.000
Ca						1.000			1.000
Na							0.239(4)		0.239
H_2O									
*H*1								1	1.000
*H*2								1	1.000
Sum	3.000		0.761	0.865	1.373	1.000	0.239	2.000	9.239
Form.	6.000		1.523	1.731	2.746	2.000	0.477	4.000	18.477
wt%	45.041		12.862	13.153	11.707	11.863	1.564	3.811	100.000
Second crystal									
*P*1	1								1.000
*P*2	1								1.000
*P*3	1								1.000
*M*1		0.316(3)	0.084	0.232	0.684				1.000
*M*2		0.684(3)	0.684		0.316				1.000
*M*3		0.657(3)		0.657	0.343				1.000
Ca						1			1.000
Na							0.231(3)		0.231
H_2O									
*H*1								1	1.000
*H*2								1	1.000
Sum	3.000		0.769	0.889	1.342	1.000	0.231	2.000	9.231
Form.	6.000		1.537	1.778	2.685	2.000	0.463	4.000	18.463
wt%	44.964		12.959	13.490	11.426	11.843	1.515	3.804	100.000

The occupancies quoted are the ratio of the number of atoms in a given site per unit cell to the multiplicity of the general position. Standard deviations of refined values are given in parentheses. Small discrepancies between entries are due to rounding off. Form.: formula; wt%: wt% oxide.

Individual spot-analyses of tassieite also gave highly variable Y and Yb contents. It appears that in some cases a portion of Y and Yb could have been contributed by xenotime-(Y) inclusions (Figs. 3a, b) intersected by the electron beam, and for this reason analytical results given in Table 9 and used in preparing compositional plots (Fig. 5) are averages from which the most yttrian compositions were removed. The cutoff ranged from 0.3 to 0.9 wt.% Y_2O_3; only two grains were not culled (*e.g.*, area 8, Table 9). Resulting average Y_2O_3 and Yb_2O_3 contents of individual grains range from 0.02 ± 0.02 to 0.66 ± 0.12 wt.%, and from 0.0 ± 0.10 to 0.15 ± 0.12 wt.%, respectively.

The major compositional variations can be expressed in terms of two substitutions consistent with the crystal-structure refinements (modified from Galliski *et al.* 1999):

$$^{Na}\square + {}^{M1,M2}Fe^{3+} = {}^{Na}Na + {}^{M1,M2}(Mg,Fe^{2+})$$

$$Mg = Fe^{2+}$$

The two substitutions are not correlated (Fig. 5b).

The Gladstone–Dale relation (Mandarino 1981) gives for crystal #2 a compatibility index $1 - (K_P/K_C)$ = 0.011 (superior).

TABLE 8. BOND LENGTHS IN TASSIEITE (Å)

	Crystal #1	Crystal #2		Crystal #1	Crystal #2
P1 - O2	1.524(3)	1.521(2)	P2 - O6	1.529(3)	1.525(3)
O1	1.532(2)	1.528(2)	O7	1.540(3)	1.533(3)
O4	1.538(2)	1.533(3)	O5	1.538(2)	1.535(3)
O3	1.540(3)	1.539(3)	O8	1.540(2)	1.539(2)
<P1- O>	1.534	1.530	<P2- O>	1.537	1.533
P3 - O12	1.539(3)	1.537(3)	*M*1 - O6	2.043(3)	2.038(3)
O9	1.540(3)	1.537(3)	O1	2.048(3)	2.047(2)
O10	1.541(3)	1.541(2)	O5	2.074(3)	2.075(3)
O11	1.543(3)	1.542(3)	O3	2.086(2)	2.088(2)
<P3- O>	1.541	1.539	O9	2.214(2)	2.213(3)
			O10	2.216(2)	2.214(3)
*M*2 - O8	1.954(2)	1.960(2)	<*M*1-O>	2.113	2.113
O12	1.966(2)	1.961(2)			
O4	2.028(3)	2.026(3)	*M*3 - O2	2.050(3)	2.045(3)
O11	2.030(2)	2.029(2)	O7	2.073(3)	2.075(3)
O3	2.043(3)	2.045(3)	OW	2.093(3)	2.096(3)
O5	2.095(2)	2.096(2)	O1	2.120(2)	2.123(2)
<*M*2-O>	2.019	2.020	O10	2.325(3)	2.326(2)
			O9	2.394(3)	2.397(3)
Ca - O11	2.399(2)	2.400(3)	<*M*3-O>	2.176	2.177
O6	2.391(3)	2.401(3)			
O4	2.470(2)	2.478(2)	Na - O7	2.127(3)	2.129(3)
O2	2.511(3)	2.511(3)	O7	2.127(3)	2.129(3)
O7	2.528(3)	2.533(3)	O12	2.563(2)	2.565(2)
O9	2.527(3)	2.536(3)	O12	2.563(2)	2.565(2)
OW	2.641(3)	2.639(3)	O2	2.670(3)	2.678(3)
O10	2.665(3)	2.666(3)	O2	2.670(3)	2.678(3)
O12	2.754(3)	2.760(3)	<Na- O>	2.453	2.457
<Ca- O>	2.543	2.547			
			H1 - Ow	0.96(8)	0.75(4)
			H2 - Ow	1.07(6)	0.94(7)

TASSIEITE: NOMENCLATURE ISSUES

There are currently two recognized phosphate species in the wicksite group; tassieite would be the third (Table 10). In addition, Peacor *et al*. (1985) and Ek & Nysten (1990) have reported "wicksite-like" minerals that appear to be closer to bederite than to wicksite in composition. In introducing bederite as a new species in the wicksite group, Galliski *et al*. (1999) argued that bederite is distinct from wicksite not only because of the homovalent Mn substitution for Fe^{2+} at *M*1 and *M*3, but also because of the heterovalent substitution $^{Na}\square + {}^{M2}Fe^{3+} = {}^{Na}Na + {}^{M2}Mg$ (Table 10). However, they did not cite the "wicksite-like" minerals from Hålsjöberg, Sweden (Ek & Nysten 1990). The two samples richest in Fe^{2+} (anal. 6 and 7) have $Fe^{2+}/(Fe^{2+} + Mn) = 0.47–0.48$ (Ek's & Nysten's data based on Fe^{2+} determinations using Mössbauer spectroscopy) or 0.50–0.55 (Fe^{2+} estimated from stoichiometry using formulae normalized to 14 cations for 24 atoms of oxygen, as was done for tassieite) and Na = 0.026–0.029 *apfu*. These two compositions imply that there could a Fe^{2+}-dominant wicksite-group mineral in which the Na site is largely vacant, *i.e.,* the Fe^{2+}-dominant analogue of bederite.

We proposed tassieite as an Na-dominant species to the CNMMN, that is, with $NaCa_2(Mg_2)(Fe^{3+}Mg)_{\Sigma 2}(Fe^{2+})_2(PO_4)_6 \bullet 2H_2O$ as the dominant end-member. Tassieite can be distinguished from wicksite and bederite either by the dominance of Mg at *M*1 or by the dominance Mg among octahedrally coordinated divalent cations (Table 10, Fig. 5a). A structure refinement would not be needed to identify a given specimen using the second criterion; Fe^{2+} could be calculated from stoichiometry. All but one of the analyzed grains in sample 113002A meet the second criterion for tassieite; this grain is wicksite with an $Mg / (Mg + Fe^{2+} + Mn^{2+})$ at *M*1–3 of 0.445 and Na = 0.56 *apfu*.

However, tassieite also has a variable Na content (Fig. 5b); most analyses give Na > □ at the Na site (tassieite), but one EMPA and the structure refinements give □ > Na, a potentially distinct species (unnamed, Table 10). Eventually, it might be possible to distinguish a Na-dominant subgroup and vacancy-dominant subgroup in the wicksite group, but for now, the most practical criterion for distinguishing tassieite, wicksite and bederite is the relative proportion of Mg, Mn and Fe^{2+} at the *M*1, *M*2 and *M*3 sites considered together; *i.e*., these minerals are related by homovalent substitutions at the *M* sites. These are rare minerals, and we do not think further refinement of the nomenclature is justified until a larger set of crystallographic and compositional data on more samples has become available.

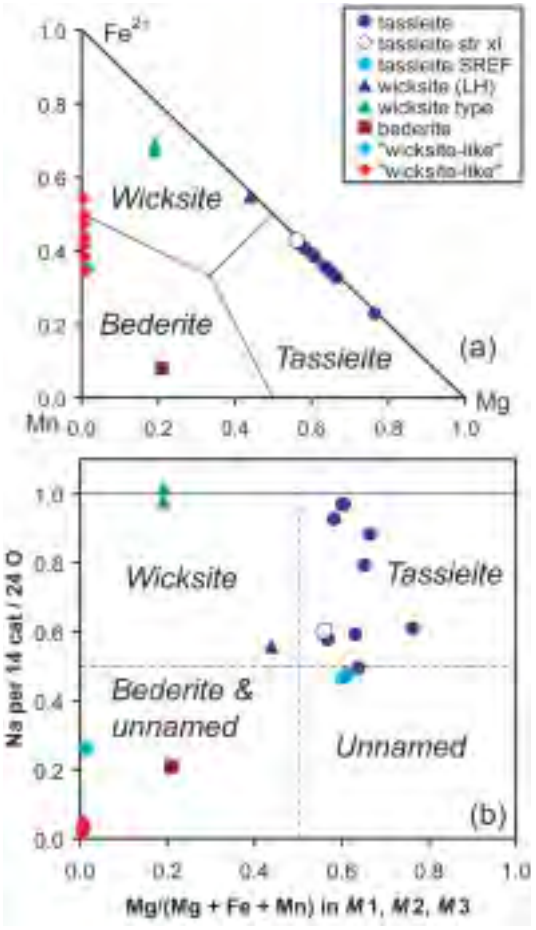

FIG. 5. Plots of wicksite-group phosphates using formulae calculated on a 14 cation per 24 oxygen basis. (a) The proportions of divalent cations at the three *M* sites considered together. Only named species are indicated. (b) The relationship between Na and the proportion of Mg at the three *M* sites considered together. Two fields are labeled "unnamed" because there are compositions or possible compositions corresponding to these two unnamed species (Table 10). Explanation and sources: tassieite: this study, tassieite str xl: electron-microprobe data for crystal #2 used in the determination of the structure (Table 9), tassieite SREF: compositions from crystal-structure refinements (Table 7); wicksite (LH): Larsemann Hills (Table 9), wicksite type: Sturman *et al*. (1981), Cooper & Hawthorne (1997); bederite: Galliski *et al*. (1999); "wicksite-like" (blue): from Bull Moose mine, South Dakota, U.S.A. (Peacor *et al*. 1985); "wicksite-like" (red): from Hålsjöberg kyanite–phosphate deposit (Ek & Nysten 1990).

TABLE 9. SELECTED COMPOSITIONS OF TASSIEITE AND WICKSITE IN SAMPLE 113002A

Grain	2nd xl	2nd xl	2nd xl*	area 1	area 3-1	area 5	area 8	area 9
method	SREF-1	SREF-2	EMPA	EMPA	EMPA	EMPA	EMPA	EMPA
No. spots	–	–	8	13	14	6	20	11
SiO_2 wt%	–	–	0.01	0.01	b.d.	b.d.	b.d.	b.d.
P_2O_5	44.96	44.97	44.54	44.64	44.96	45.34	45.88	46.72
SO_3	–	–	0.06	b.d.	0.30	0.04	0.04	0.02
MgO	11.43	10.83	10.95	8.60	14.16	13.21	12.61	15.99
MnO	–	–	0.38	0.49	0.31	0.30	0.30	0.24
FeO_{meas}	25.15	25.15	25.40	27.75	19.23	20.05	22.14	17.03
FeO_{calc}	13.49	12.43	14.93	19.12	12.39	15.27	12.42	8.57
$Fe_2O_{3\ calc}$	12.96	14.14	11.63	9.60	7.61	5.32	10.80	9.40
Na_2O	1.51	1.97	1.96	1.78	2.88	3.14	1.63	2.05
CaO	11.84	11.84	11.56	11.76	11.79	11.70	12.20	12.01
SrO	–	–	0.02	0.01	0.04	b.d.	0.07	0.01
Y_2O_3	–	–	0.26	0.05	0.44	0.36	0.02	0.63
La_2O_3	–	–	b.d.	b.d.	0.02	0.02	b.d.	0.01
Ce_2O_3	–	–	0.08	b.d.	0.02	0.03	0.03	b.d.
Nd_2O_3	–	–	b.d.	0.02	0.02	0.02	b.d.	0.01
Yb_2O_3	–	–	0.13	0.01	0.07	0.10	b.d.	0.09
UO_2	–	–	0.04	0.04	b.d.	0.01	b.d.	0.04
F	–	–	0.04	b.d.	0.04	0.03	b.d.	0.02
Cl	–	–	b.d.	b.d.	0.02	b.d.	b.d.	0.01
H_2O_{calc}	3.80	3.81	3.78	3.72	3.80	3.77	3.84	3.90
Sum	100.00	100.00	100.34	99.85	98.81	98.64	99.84	99.71
Si *apfu*	–	–	0.001	0.001	0.000	0.000	0.000	0.000
P	6.000	6.000	5.981	6.089	6.009	6.111	6.071	6.077
S	–	–	0.007	0.000	0.036	0.005	0.005	0.003
Sum *P*	6.000	6.000	5.989	6.091	6.045	6.116	6.076	6.080
Mg	2.685	2.545	2.589	2.066	3.333	3.136	2.938	3.663
Mn	–	–	0.051	0.066	0.042	0.041	0.039	0.031
Fe^{2+}	1.778	1.638	1.981	2.576	1.635	2.034	1.624	1.102
Fe^{3+}	1.537	1.677	1.389	1.163	0.904	0.637	1.270	1.087
Na	–	0.140	–	–	–	–	–	–
Sum *M*	6.000	6.000	6.010	5.872	5.914	5.847	5.871	5.883
Na	0.463	0.463	0.603	0.557	0.882	0.969	0.494	0.610
Ca	2.000	2.000	1.964	2.029	1.994	1.996	2.043	1.978
Sr	–	–	0.002	0.001	0.004	0.000	0.007	0.001
Sum *Ca*	2.000	2.000	1.966	2.030	1.997	1.996	2.050	1.979
Y	–	–	0.022	0.004	0.037	0.031	0.002	0.052
La	–	–	0.000	0.000	0.001	0.001	0.000	0.001
Ce	–	–	0.005	0.000	0.001	0.002	0.002	0.000
Nd	–	–	0.000	0.001	0.001	0.001	0.000	0.001
Yb	–	–	0.006	0.000	0.003	0.005	0.000	0.004
U	–	–	0.002	0.001	0.000	0.001	0.000	0.001
Sum cations	14.463	14.463	14.603	14.557	14.882	14.969	14.494	14.610
H_2O	4.000	4.000	4.000	4.000	4.000	4.000	4.000	4.000
X_{Mg}	0.602	0.608	0.567	0.445	0.671	0.607	0.644	0.769

SREF-1: single-crystal refinement of the structure assuming no Na in *M*3. SREF-2: the same, but assuming total Na = Na established by electron-microprobe analysis (EMPA). No. spots: number of spots where elements were counted for 5 s. b.d.: below detection. * Average result of two electron-microprobe analyses at 6 and 2 spots. Sums do not include measured FeO, F or Cl. Note that Al, Ti, Tm are below limit of detection (Tm not sought in second crystal). The formulae and Fe^{3+}:Fe^{2+} ratio are calculated assuming total cations – Na = 14 *apfu*, and 24 O (anhydrous basis). H_2O is calculated assuming 4 H_2O per formula unit. X_{Mg} = Mg/(Mg + Fe^{2+}).

TABLE 10. POPULATIONS OF CRITICAL SITES IN PHOSPHATE END-MEMBERS OF THE WICKSITE GROUP

Site	*Na*	*M*1	*M*2	*M*3
Wicksite	Na	Fe^{2+}_2	$Fe^{3+}Mg$	Fe^{2+}_2
Unnamed*	□	Fe^{2+}_2	Fe^{3+}_2	Mn^{2+}_2
Unnamed	Na	Mn^{2+}_2	$Fe^{3+}Mg$	Mn^{2+}_2
Bederite	□	Mn^{2+}_2	Fe^{3+}_2	Mn^{2+}_2
Tassieite†	Na	Mg^{2+}_2	$Fe^{3+}Mg$	Fe^{2+}_2
Unnamed	□	Mg^{2+}_2	Fe^{3+}_2	Fe^{2+}_2

Modified from Galliski *et al.* (1999). * Possible end-member implicit in Fe^{2+}-rich "wicksite-like" minerals reported by Ek & Nysten (1990). † Defined as the end member of tassieite.

Acknowledgements

We thank Frédéric Hatert and Ştefan Marincea for their constructive reviews and André-Mathieu Fransolet and Robert F. Martin for their expert editing. We also wish to thank the leader, Bob Jones, and other members of the 2003–2004 Australian National Antarctic Research Expedition for logistical support during the summer field season. The fieldwork of CJC and ESG in the Larsemann Hills was supported by Antarctic Science Advisory Committee Project no. 2350. The research of ESG and MGY was supported by U.S. National Science Foundation grants OPP–0228842 and MRI–0116235 to the University of Maine.

References

Autefage, F. (1980): Variations de la teneur en sodium et en potassium dans des minéraux au cours de leur analyse à la microsonde électronique. *Bull. Minéral.* **103**, 48-53.

Autefage, F. & Couderc, J.-J. (1980): Étude du mécanisme de la migration du sodium et du potassium au cours de leur analyse à la microsonde électronique. *Bull. Minéral.* **103**, 623-629.

Bianchi, R., Pilati, T. & Mannucci, G. (1987): Crystal structure of grischunite. *Am. Mineral.* **72**, 1225-1229.

Carson, C.J., Dirks, P.H.G.M., Hand, M., Sims, J.P. & Wilson, C.J.L. (1995b): Compressional and extensional tectonics in low–medium pressure granulites from the Larsemann Hills, East Antarctica. *Geol. Mag.* **132**, 151-170.

Carson, C.J., Hand, M. & Dirks, P.H.G.M. (1995a): Stable coexistence of grandidierite and kornerupine during medium pressure granulite facies metamorphism. *Mineral. Mag.* **59**, 327-339.

COOPER, M.A. & HAWTHORNE, F.C. (1997): The crystal structure of wicksite. *Can. Mineral.* **35**, 777-784.

DIRKS, P.H.G.M., CARSON, C.J. & WILSON, C.J.L. (1993): The deformational history of the Larsemann Hills, Prydz Bay: the importance of the Pan-African (500 Ma) in East Antarctica. *Antarctic Sci.* **5**, 179-192.

EK, R. & NYSTEN, P. (1990): Phosphate mineralogy of the Hålsjöberg and Hökensås kyanite deposits. *Geol. Fören. Stockholm Förh.* **112**, 9-18.

FRANSOLET, A.-M. (1973): La mélonjosephite $CaFe^{2+}Fe^{3+}(PO_4)_2(OH)$, une nouvelle espèce minérale. *Bull. Soc. fr. Minéral. Cristallogr.* **96**, 135-142.

FRANSOLET, A.-M., ABRAHAM, K. & SPEETJENS, J.-M. (1985): Evolution génétique et signification des associations de phosphates de la pegmatite d'Angarf-Sud, plaine de Tazenakht, Anti-Atlas, Maroc. *Bull. Minéral.* **108**, 551-574.

GALLISKI, M.A., COOPER, M.A., HAWTHORNE, F.C. & ČERNÝ, P. (1999): Bederite, a new pegmatite phosphate mineral from Nevados de Palermo, Argentina: description and crystal structure. *Am. Mineral.* **84**, 1674-1679.

GRAESER, S., SCHWANDER, H. & SUHNER, B. (1984): Grischunit ($CaMn_2[AsO_4]_2$), eine neue Mineralart aus den Schweizer Alpen; zur Mn–As-Mineralisation des Oberhalbstein-Gebietes (I). *Schweiz. Mineral. Petrogr. Mitt.* **64**, 1-10.

GREW, E.S., ARMBRUSTER, T., MEDENBACH, O., YATES, M.G. & CARSON, C.J. (2006): Stornesite-(Y), $(Y,Ca)\square_2Na_6(Ca,Na)_8(Mg,Fe)_{43}(PO_4)_{36}$, the first terrestrial Mg-dominant member of the fillowite group, from granulite-facies paragneiss in the Larsemann Hills, Prydz Bay, East Antarctica. *Am. Mineral.* **91**, 1412-1424.

MANDARINO, J.A. (1981): The Gladstone – Dale relationship. IV. The compatibility concept and its application. *Can. Mineral.* **19**, 441-450.

MEDENBACH, O. (1985): A new microrefractometer spindle-stage and its application. *Fortschr. Mineral.* **63**, 111-133.

MERLET, C. (1994): An accurate computer correction program for quantitative electron-probe microanalysis. *Mikrochim. Acta* **114**, 363-376.

MOORE, P.B. (1974): I. Jahnsite, segelerite, and robertsite, three new transition metal phosphate species. II. Redefinition of overite, an isotype of segelerite. III. Isotypy of robertsite, mitridatite, and arseniosiderite. *Am. Mineral.* **59**, 48-59.

OBERTI, R., HAWTHORNE, F.C., UNGARETTI, L. & CANNILLO, E. (1993): The behaviour of Mn in amphiboles: Mn in richterite. *Eur. J. Mineral.* **5**, 43-51.

PEACOR, D.R., DUNN, P.J., RAMIK, R.A., CAMPBELL, T.J. & ROBERTS, W.L. (1985): A wicksite-like mineral from the Bull Moose mine, South Dakota. *Can. Mineral.* **23**, 247-249.

POVONDRA, P., PIVEC, E., ČECH, F., LANG, M., NOVÁK, F., PRACHAŘ, I. & ULRYCH, J. (1987): Přibyslavice peraluminous granite. *Acta Univ. Carol., Geol.* **3**, 183-283.

REN, L., GREW, E.S., XIONG, M. & MA, Z. (2003): Wagnerite-*Ma5bc*, a new polytype of $Mg_2(PO_4)(F,OH)$, from granulite-facies paragneiss, Larsemann Hills, Prydz Bay, East Antarctica. *Can. Mineral.* **41**, 393-411.

ROBERTSON, B.T. (1982): Occurrence of epigenetic phosphate minerals in a phosphatic iron-formation, Yukon Territory. *Can. Mineral.* **20**, 177-187.

ROBINSON, G.W., VELTHUIZEN, J., ANSELL, H.G. & STURMAN, B.D. (1992): Mineralogy of the Rapid Creek and Big Fish River area, Yukon Territory. *Mineral. Rec.* **23**, 1-47.

SHELDRICK, G.M. (1997): SHELXL–97, *Program for Refinement of Crystal Structures*. University of Göttingen, Göttingen, Germany.

STURMAN, B.D., PEACOR, D.R. & DUNN, P.J. (1981): Wicksite, a new mineral from northeastern Yukon Territory. *Can. Mineral.* **19**, 377-380.

STÜWE, K., BRAUN, H.-M. & PEER, H. (1989): Geology and structure of the Larsemann Hills area, Prydz Bay, East Antarctica. *Aust. J. Earth Sci.* **36**, 219-241.

YVON, K., JEITSCHKO, W. & PARTHE, E. (1977): LAZY PULVERIX, a computer program for calculating X-ray and neutron diffractiion powder patterns. *J. Appl. Crystallogr.* **10**, 73-74.

Received February 1, 2006; revised manuscript accepted June 23, 2006.